香港浸會大學
HONG KONG BAPTIST UNIVERSITY

HKBU Scholars

Using Ultralow Dosages of Electron Acceptor to Reveal the Early Stage Donor–Acceptor Electronic Interactions in Bulk Heterojunction Blends

Ho, Carr Hoi Yi; Cheung, Sin Hang; Li, Ho-Wa; Chiu, Ka Lok; Cheng, Yuanhang; Yin, Hang; Chan, Mau Hing; So, Franky; Tsang, Sai-Wing; So, Shu Kong

Published in:
Advanced Energy Materials

DOI:
10.1002/aenm.201602360

Published: 21/06/2017

Document Version:
Peer reviewed version

Link to publication

Citation for published version (APA):
Ho, C. H. Y., Cheung, S. H., Li, H.-W., Chiu, K. L., Cheng, Y., Yin, H., Chan, M. H., So, F., Tsang, S.-W., & So, S. K. (2017). Using Ultralow Dosages of Electron Acceptor to Reveal the Early Stage Donor–Acceptor Electronic Interactions in Bulk Heterojunction Blends. *Advanced Energy Materials*, *7*(12), Article 1602360. https://doi.org/10.1002/aenm.201602360

General rights
Copyright and intellectual property rights for the publications made accessible in HKBU Scholars are retained by the authors and/or other copyright owners. In addition to the restrictions prescribed by the Copyright Ordinance of Hong Kong, all users and readers must also observe the following terms of use:

- Users may download and print one copy of any publication from HKBU Scholars for the purpose of private study or research
- Users cannot further distribute the material or use it for any profit-making activity or commercial gain
- To share publications in HKBU Scholars with others, users are welcome to freely distribute the permanent publication URLs

Downloaded on: 17 Apr, 2025

Authors

Carr Hoi Yi Ho, Sin Hang Cheung, Ho-Wa Li, Ka Lok Chiu, Yuanhang Cheng, Hang Yin, Mau Hing Chan, Franky So, Sai-Wing Tsang, and Shu Kong So

This journal article is available at HKBU Institutional Repository: https://repository.hkbu.edu.hk/hkbu_staff_publication/6415

DOI: 10.1002/aenm.201602360
Article type: Full Paper

Title: Using Ultra-Low Dosages of Electron Acceptor to Reveal the Early Stage Donor-Acceptor Electronic Interactions in Bulk Heterojunction Blends

*Carr Hoi Yi Ho, Sin Hang Cheung, Ho-Wa Li, Ka Lok Chiu, Yuanhang Cheng, Hang Yin, Mau Hing Chan, Franky So, Sai-Wing Tsang, Shu Kong So**

C. H. Y. Ho, S. H. Cheung, K. L. Chiu, H. Yin, Dr. M. H. Chan, Prof. S. K. So
Department of Physics and Institute of Advanced Materials,
Hong Kong Baptist University,
Kowloon Tong, Hong Kong,
People's Republic of China
E-mail: skso@hkbu.edu.hk

H.-W. Li, Y. Cheng, Dr. S.-W. Tsang
Department of Physics and Materials Science,
City University of Hong Kong,
Kowloon Tong, Hong Kong,
People's Republic of China

Prof. F. So
Department of Materials Science and Engineering,
North Carolina State University, Raleigh, NC 27606,
United States of America

Keywords: (bulk heterojunction, traps, photothermal deflection spectroscopy, carrier transport, photovoltaic)

Tuning the donor-acceptor (D-A) weight ratio is an essential step to optimize the performance of a bulk heterojunction (BHJ) solar cell. The un-optimized regime with a low acceptor concentration is generally unexplored despite it may reveal the early stage electronic D-A interactions. In this study, PTB7:$PC_{71}BM$ is used to examine factors that limit the device performance in un-optimized regime. The key limiting factor is the creation of traps and localized states originated from fullerene molecules. Photothermal deflection spectroscopy (PDS) is used to quantify the trap density. Starting with pristine PTB7, addition of small concentration of fullerene increases the electron trap density and lowers the electron mobility. When the D-A weight ratio reaches 1 : 0.1, fullerene percolation occurs. There is an abrupt drop in trap density and simultaneously a six orders of magnitude increase in the electron mobility. Furthermore, the fill factors of the corresponding photovolatic devices are found to

anti-correlate with the trap density. This study reveals that electron trapping is the key limiting factor for un-optimized BHJ solar cells in low fullerene regime.

1. Introduction

Organic photovoltaic (OPV) is an emerging renewable energy technology. With the use of nontoxic organic materials, one can fabricate light, flexible, low-cost devices, and have good performance in low light conditions.[1-3] The active layer of an OPV device, which converts absorbed light energy into electrical energy, is usually prepared in the form of bulk-heterojunction (BHJ).[4] In most of the OPV cells, the BHJ includes a blend of electron-donating polymer and electron-accepting fullerene with a suitable weight ratio. The BHJ approach provides a much larger donor-acceptor (D-A) interface when compared to bilayer device architecture. Furthermore, polymer and fullerene domains are formed on tens of nanometers length scale.[5] The BHJ morphology plays important roles in both exciton dissociation and charge transport processes.[6] Once the active layer absorbed light, excitons are dissociated at the D-A interface to generate delocalized holes and electrons, which would hop throughout the favorable transport sites in the donor and the acceptor domains, respectively, and finally reach their corresponding electrodes to generate electricity.

In order to obtain an optimized BHJ morphology, different strategies such as tuning the D-A weight ratio, annealing the as-cast active layer with different temperatures and solvents, using high boiling point solvent additive with selective solubility, have been investigated and employed extensively.[7-10] In general, a good BHJ morphology should fulfill several criteria: compositionally graded in vertical direction for charge collection, suitable domain size for exciton dissociation, and favorable molecular orientation for charge transport.[11-13] Within all this possible strategies, tuning D-A weight ratio should be the most important and primary

process during OPV devices fabrication. Yet the rule remains to be clearly established and it is usually done on a trial-and-error basis.[14-17] The composition dependence of carrier transport in polymer: fullerene BHJ films was initially reported by Brabec et al.[14] By time-of-flight photocurrent measurements, they revealed that the electron and hole mobilities strongly dependent on the acceptor concentration. Chirvase et al. then studied the role of composite weight ratio in poly(3-hexylthiophene) : [6,6]-phenyl-C61 butyric acid methyl ester (P3HT : PCBM) BHJ solar cells.[15] It was observed that the variation of PCBM cluster size is correlated with its concentration in the BHJ blend. The growth of the PCBM clusters leads to the formation of percolation paths for charge transport and thus improves the photocurrent. Since then, the correlation between photovoltaic properties and D-A weight ratios has been investigated and reported by different groups.[6, 16-21] In a recent report by Hou et al., the effect of D-A weight ratio on a high efficiency BHJ, namely PIDTDTQx : $PC_{71}BM$ was analyzed.[21] The change of OPV device performances, carrier mobility and surface morphology were demonstrated. They proposed that the ambipolar charge transport characteristics of $PC_{71}BM$ play an important role on charge transport. Also a balanced mobility between electrons and holes is the key to obtain a good fill factor in OPV cells. A comprehensive understanding is lacking so far for the evolution of BHJ, specifically, how the percolation pathway is formed as $PC_{71}BM$ is introduced into the polymer matrix.[22-23] The common strategy to optimize the blend composition is to establish a balanced charge transport. The question is whether a balanced charge transport is sufficient for an optimum solar cell.

In this report, poly{4,8-bis[(2-ethylhexyl)oxy]benzo[1,2-b:4,5-b']dithiophene-2,6-diyl-alt-3-fluoro-2-[(2-ethylhexyl)carbonyl]thieno[3,4-b]thiophene-4,6-diyl}:(6,6)-phenyl C71 butyric acid methyl ester (PTB7:$PC_{71}BM$) BHJ is chosen for investigation. This BHJ is one of the most common and efficient materials used. With appropriate interlayers and a suitable solvent additive, a power conversion efficiency (PCE) as high as 10.1% can be achieved.[24] In this

paper we investigate the impact of D-A weight ratio on the performance of PTB7:$PC_{71}BM$ BHJ OPV cells. With ultra-low dosages of acceptor (~0.1 wt%) added into PTB7, we reveal the early stage of electronic process between donor and acceptor. Three distinct regimes can be uncovered with respect to the fullerene content. We therefore performed carrier transport measurements in these three regimes for correlating device performances to transport parameters. The data indicate that the reduction of electron traps is the main factor that abruptly changes the charge transport during the percolation of fullerene domains. With photothermal deflection spectroscopy (PDS), subgap optical absorption spectra of the BHJ with different D-A weight ratios were investigated. It is observed that the trap density is anti-correlated with the fill factor (FF) in all three regimes and a low electron trap density is the key to obtain a high fill factor. Considering the observations, we propose that $PC_{71}BM$ molecules trend to intercalate with PTB7 instead of self-aggregates in the early state of BHJ formation. These results provide insights into the BHJ formation, a full picture of charge transport dynamics and new avenue to improve the photovoltaic performances of OPV devices**.**

2. Results and Discussion

2.1. Effect of Donor : Acceptor Weight Ratio on Organic Photovoltaic Device Performance

Organic photovoltaic (OPV) devices with a structure of ITO/PEDOT:PSS/PTB7:$PC_{71}BM$ /LiF/Al were fabricated to investigate the photovoltaic properties at different D-A weight ratios. In such a system, PTB7 acts as the electron donor while $PC_{71}BM$ acts as the electron acceptor. (Chemical structures can be found in **Figure S1**) The thickness of the active layer for each device was about 100 nm. **Figure 1** summarized the device performances under the

illumination of AM 1.5G, 100 mW/cm^2. (All current-voltage characteristics and external quantum efficiencies (EQE) are shown in **Figure S4** and **Figure S5** respectively) In general, the open circuit voltage (V_{oc}) monotonically decreases with increasing fullerene content, ranging from 1.21 V to 0.67 V. In contrast, distinct peaks were observed for the short circuit current density (J_{sc}), the fill factor (FF), and in the power conversion efficiency (PCE), and these three parameters are correlated. For each parameter, three regimes can be identified: ***(Regime I)*** For a polymer : fullerene weight ratio less than 1 : 0.1, J_{sc} increases gradually from 0.13 to 0.61 *mA cm*$^{-2}$, and the PCE remains well under 0.1%. It should be noted that FF of pure PTB7 device is 35%, but when a small amount of fullerene, even one per thousand of content is added, the FF drops quickly to 25% and persists through this regime. ***(Regime II)*** Further increase of the fullerene content leads to abrupt increases in $J_{sc,}$ FF and PCE, to their optimized values (J_{sc} = 17.0 mA/cm^{2}V^{-1}s$^{-1,}$ FF = 67% and PCE = 8.4%) at 1 : 1.5 D-A weight ratio. ***(Regime III)*** Beyond the optimized D-A weight ratio of 1 : 1.5, more $PC_{71}BM$ produces negative effects on the $J_{sc,}$ FF and PCE. These three parameters drops monotonically as the fullerene content further increases. For the pure fullerene OPV cell, only a PCE of 0.029% can be obtained, which can be compared to the PCE of 0.054% for a pure polymer cell. The values of J_{sc}, V_{oc}, FF and PCE can be found in **Table 1**.

2.2. Electron and hole transport properties at different donor-acceptor weight ratios

To probe the charge transport properties of the blend films with different D-A weight ratios, space-charge-limited-current (SCLC) model with traps was used to measure the zero-field electron mobility in electron-only devices. The device structure ITO/Al/PTB7:$PC_{71}BM$/LiF/Al was used to measure the current-voltage characteristics of BHJ films. The LiF/Al act as cathode while the opposite Al layer act as hole-blocking but electron

transporting layer. Electric-field dependent current of the samples were measured and carrier mobilities were extracted using following equation:

$$J_{SCL}\, d = \frac{9}{8}\varepsilon_0\varepsilon_r\mu_0\theta\, exp\left(0.89\beta\sqrt{F}\right)F^2 \quad (1)$$

where J_{SCL} is the space-charged-limited current density, d is the thickness of tested layer, ε_0 is the permittivity of vacuum, ε_r is the relative permittivity of the polymer, θ defines the fraction of trapped carriers, μ_0 is the zero-field mobility, β is the field-dependent coefficient, and F is the average electrical field applied on the sample.[25-27]

The $PC_{71}BM$ content dependency of electron mobility at room temperature is shown in **Figure 2**. Consistent with OPV device performances, the data also can be divided into three distinct regimes: ***(Regime I)*** Electron mobility of pure PTB7 is 9.0×10^{-9} $cm^2V^{-1}s^{-1}$. Upon adding small amount of fullerene, the electron mobility dropped around two orders of magnitude to 1.1×10^{-10} $cm^2V^{-1}s^{-1}$ at relative fullerene ratio 0.1. Instead of promoting electron transport, fullerene molecules under a low concentration suppress the electron mobility. ***(Regime II)*** From D-A weight ratio 1 : 0.1 to 1 : 1.5, the mobility monotonically increase by six orders of magnitudes with the $PC_{71}BM$ content. At a D:A ratio of 1 : 1.5, the electron mobility reaches 2.2×10^{-4} $cm^2V^{-1}s^{-1}$. This indicates that the electron transport pathway undergoes percolation. ***(Regime III)*** At higher $PC_{71}BM$ contents the electron mobility practically saturated in the order of 10^{-4} $cm^2V^{-1}s^{-1}$, and reaching the ultimate value of 9.7×10^{-4} $cm^2V^{-1}s^{-1}$ for pure fullerene. The value is consistent with that reported by Blom et al.[28] Besides electron mobilities, we also constructed hole-only devices as shown in **Figure S2.** In such a structure, PEDOT:PSS acts as the hole injection contact, while the thin layer of spiro-TPD:CuPc acts as the electron blocking and trapping (EBT) layer to prevent electron leakage from the Au cathode.[29] The zero-field hole mobility of pure PTB7 is 2.8×10^{-4} $cm^2V^{-1}s^{-1}$, which is comparable to the value reported by Yu et al. and our pervious results.[12,30] Adding

fullerene into BHJ film only shows small impact on hole mobility, which is within the range between 10^{-4} - 10^{-5} $cm^2V^{-1}s^{-1}$. From Figure 2, we can see that the variations of electron and hole mobilities with the D-A weight ratios are fundamentally different. Hole conduction paths are along or in between polymer chains like conduction rods. They are generally better connected and therefore, hole mobility vary little with the D-A weight ratios. On the other hand, electrons conduct between the fullerene domains, which can be modeled as small nano-particles. A sharp rise in electron mobility should occur when the fullerene concentration reaches the percolation threshold.

To further understand the electrical transport properties, temperature-dependent *J-V* measurements between 226 K and 327 K were carried out. Gaussian disorder model (GDM) was employed for analysis.[31] The model describes that charge carrier hop between discrete transporting sites which are energetically Gaussian distributed, and the carrier mobility depend on electric field and temperature as:

$$\mu(F,T) = \mu_\infty \, exp\left[-\left(\frac{2\sigma}{3kT}\right)^2\right] exp\left(\beta\sqrt{F}\right) \quad (2)$$

where μ_∞ is the high-temperature limit mobility, σ is the energetic disorder parameter, k is the Boltzmann constant, and T is the absolute temperature. At a low electric field, the later exponential term vanished. From a plot of zero-field mobility (μ_0) vs $(1/T)^2$, the slope can be used to extract σ and the y-intercept represents the μ_∞. The extracted σ and μ_∞ at different D-A weight ratio are plotted in **Figure 2 and S6** respectively. For electrons μ_∞ follows the same trend as μ_0. The energetic disorder of holes remains in the range of 80-90 meV, while energetic disorder of electrons shows a substantial reduction from 122 meV to 62 meV. The reduction in electrons energetic disorder reflects a distinct change on energy width of the electron hopping site manifold, which arises from interactions with its environment.[32] Using

SCLC model with traps and GDM, we conclude that electron transport is the main factor that varies at different D-A weight ratio, and well-correlated with OPV device performances.

2.3. Correlation between Subgap Optical Absorption and Fill Factors in OPV Devices

Additional insights on the formation of the BHJs can be obtained by studying their subgap optical absorptions. For a semiconducting material with an energy gap (E_g), the absorptions below E_g are generally related to traps or localized states.[33,34] To measure subgap absorptions, we employ a highly sensitive technique, known as photothermal deflection spectroscopy (PDS). Its principle of operation is well documented.[35-38] The experimental apparatus is shown in **Figure S7**.

The PDS spectra of the BHJs are shown in **Figure 4**. For clarify, we only show three PDS spectra for each regime. We observe that there is a noticeable increase in the subgap absorption after the addition of fullerene molecules, especially before their percolation. To quantify the increase in the subgap absorption, we estimate the nominal trap state density (N) of the BHJ by the optical sum rule:[39]

$$N = \frac{cnm}{2\pi^2 \hbar e^2} \int \alpha_{sub}(E)\, dE \qquad (3)$$

In **Equation (3)**, E is the photon energy, c is the speed of light, n is the refractive index, m is the effective mass of electron, e is the elementary charge, $\hbar$ is the Planck constant. α_{sub} denotes the subtracted subgap absorption by Urbach absorption. [$\alpha_{sub}(E) = \alpha(E) - \alpha_u(E)$, where $\alpha_u = \alpha_0\, exp\left(h\nu - E_g/E_u\right)$ for $E < E_g$, and E_u is the Urbach energy.][40] Such an estimation of the trap density has been widely used for the characterization solar cell materials.[33] More recently, these absorptions are also thought to be associated with charge-transfer (CT) states in BHJs. In principle, both traps and CT states can be observed by PDS. However, in the present study, before the percolated pathways of $PC_{71}BM$ has been formed in

low doping ratios, the CT states are disconnected from the charge separation (CS) states and therefore acting as electron traps to hinder the carrier transport.[41] **Figure 5** shows the change of trap densities at different D-A weight ratios. In order to highlight only the effect of fullerene, the trap density of PTB7 is taken to be zero. In the same plot, we show the FFs of OPV devices vs D-A weight ratios. One striking feature is the apparent anti-correlation between the change in trap density and the FFs of OPV devices. Especially in regime II, the trap density changes by an amount of about 1.3×10^{18} cm^{-3} while the FF improves abruptly from 24% to 67%. The order of trap density is verified by estimating the fullerene cluster size when percolation starts, as shown in Appendix. There are previous studies that also reported OPV parameters in BHJ (including FF) show the same trend with trap density in the device.[42-46]

Besides trap density, the added fullerene molecules give rise to new features in the PDS spectra. In Figure 4, starting at a D-A weight ratio of 1 : 0.5, a broad peak centered at 1.1 eV appears. A rational assignment is the energy location of localized CT states at the polymer-fullerene interface.[47] A similar and related feature is located at about 1.5 eV. Addition of more fullerenes does not affect these peak intensities, as most D-A interfaces are already occupied. These peaks only disappear at high fullerene content due to much reduced D-A interfaces. Finally, we note for the PDS spectra the occurrence of a peak at 0.9 eV. This peak is very prominent for pure $PC_{71}BM$. Its assignment is uncertain as it appears erratically. By comparing the spectrum of pure fullerene to those previously reported for polymer of BHJ, this peak may be due to the 2^{nd} vibrational overtone of the –CH stretch in $PC_{71}BM$.[48-50]

2.4. Impact of Donor : Acceptor Weight Ratios on Electron Transport Pathway Percolation

Figure 6(a-f) shows the morphological data of BHJ films from atomic force microscopy (AFM). For small fullerene content, the surface is smooth, with a roughness of around 0.6 nm, indicating that $PC_{71}BM$ fully intercalates into the PTB7 backbone. When the fullerene content reached the same amount as polymer, they form large domain aggregations, in the size of 10-100 nm, and increase surface roughness, implied that the percolation of electron pathway in fullerene. Recently, McGehee et al. purposed that the fullerene tends to dock with sterically accessible acceptor moiety (Thienothiophene (TT) unit) of the donor-acceptor copolymer PTB7, while the donor moiety (Benzodithiophene (BDT) unit) is sterically hindered due to the branched alkyl substituents.[51] A simplified illustration can be found in **Figure 7**. Combining the observations from carrier transport measurements, photothermal deflection spectroscopy, and morphological analysis, we hereby proposed that the "docking interaction" is driven by interaction between PTB7 and $PC_{71}BM$. When small amount of fullerene is added into the BHJ, instead of forming aggregation, the fullerene tends to dock with TT unit of PTB7, until all the available seats are occupied. Once the fullerene cannot find the place to dock, they start to aggregate and connect together, percolate into a complete electron transport pathway. **Figure 6(g)** shows the schematic diagram of how electron transport pathway percolates with fullerene content, in the means of transport energies and transport sites. For clarify, we only show the lowest unoccupied molecular orbitals for PTB7 and $PC_{71}BM$. Without any fullerene, the electron conduction primarily occurs in the polymer sites. For fullerene concentration below its percolation threshold, the fullerene molecules dock to the TT unit of PTB7, serve as electron traps instead of promoting electron transport. A simplified model is shown in **Figure 7**. When fullerene content are high enough, they start to aggregate and percolation occurs, facilitates the electron transport in a lower energy level.

The mixing dynamics and percolation between PTB7 and $PC_{71}BM$ was further supported by the steady-state photoluminescence, as shown in **Figure 8**. The peak around 770 nm (≈1.6 eV) is the PL emission peak of PTB7.[52] Upon addition of one per thousand of $PC_{71}BM$, the peak decreased significantly by two-third, meaning that the generated exciton is efficiently quenched. The emission is near completely quenched at a D-A weight ratio of 1: 0.3, indicating the well mix of polymer and fullerene. Ade et al. also observed a 70:30 wt% molecularly mixed matrix in PTB7 : $PC_{71}BM$ BHJ once the solvent additive 1,8-diiodooctane (DIO) is added,[53] which is coincide with our observed percolation threshold and argument.

3. Conclusion

A detailed investigation was carried out to study the impact of donor-acceptor weight ratio on the performance of PTB7 : $PC_{71}BM$ based OPV cells. Three distinct regimes can be uncovered in terms of the electron transport pathway evolution. Using SCLC model with traps to correlate device performances and transport parameters, we found that the hole mobility only exhibit a slight reduction as the fullerene weight fraction is increased from 0-80%. In contrast, the electron mobility exhibit three distinct regimes that correlates very well with the change in device performances. Detailed OPV parameters were further analyzed. Among them, J_{SC} tracks the PCE closely, indicating exciton dissociation and transport are the most critical factors in deciding the growth of PCEs. The unconnected fullerene domains play an important role on electron transport which they act as traps and hindered electron mobiltiy. From the photothermal deflection spectroscopy we observed that the subgap optical absorption, which is a measure of the trap density, is well anti-correlated with fill factor of OPV devices. The origin of low FF is mainly due to the electron traps and localized states from fullerenes. Based on the observations, we proposed that $PC_{71}BM$ tends to intercalate

with PTB7 backbone instead of self-aggregates. This work not only demonstrates the correlation between D-A weight ratios and BHJ device performances, but also reveals the physical origins behind the changes.

4. Experimental section

Materials: PTB7, $PC_{71}BM$, CB, DIO, Spiro-TPD, PEDOT:PSS was purchased from 1-Material, Nano-C, Sigma-Aldrich, Tokyo Chemical Industry Co., Luminescence Technology, Heraeus respectively. These materials were used as received. CuPc was purchased from Sigma-Aldrich, and was purified by sublimation before use.

OPV Cell Fabrication and Characterization: The device structure of the OPV cell was ITO/PEDOT:PSS/PTB7:$PC_{71}BM$/LiF/AL. ITO patterned glass substrate was firstly cleaned by deconex for 10 min at 120°C. The substrate was then cleaned by deionized water, acetone in ultrasonic bath followed by UV-ozone treatment. PEDOT:PSS as anode buffer layer was spin coated on the UV-treated substrate, forming a 30 nm film, followed by annealing at 140°C for 10 min in air. PTB7:$PC_{71}BM$ with different weight ratios were dissolved in chlorobenzene. 3 vol% DIO was added to the solution. The solution was stirred at 70°C overnight before filtering, then spin coated on PEDOT:PSS in a glove box to form a ~100 nm BHJ layer. The sample was annealed at 40°C in a glove box overnight, then transported into a thermal evaporator to coat LiF (1 nm) and Al (130 nm) on the BHJ layer under high vacuum. Solar cell was characterized by AM 1.5 G simulator with an intensity of 100 mW cm^{-2}.

Electron and hole mobility measurement by J-V SCLC measurements*:* The device structure is similar to the OPV device. For the electron-only devices, the PEDOT: PSS layer is replaced by a 50 nm aluminum film serving as a hole blocking layer. Before spin coating the active layer solution, a thin CB layer was spin coated firstly to promote the contact between Al and BHJ blend. For hole-only devices, after the annealing active layer overnight, the

sample was transferred to high vacuum for thermal co-evaporation of a 10 nm spiro-TPD:CuPc electron blocking and trapping layer. The coating rate of spiro-TPD and CuPc was 4.9 Å/s and 0.1 Å/s respectively. After device fabrication, the device was put in an Oxford cryostat with a pressure of less than 20 mTorr for measurement. The temperatures of the sample were regulated between 226 and 327 K.

External quantum efficiency (EQE): Measurements were conducted with home-built set-up equipped with 1000 W Xenon Arc Lamp (Newport) as light source, mono-chromator (Zolix), optical chopper (ThorLabs), lock-in amplifier (Standard Research SR830), current amplifier (Standard Research SR570) and calibrated Silicon and Germanium detectors (ThorLabs). Current amplifier and a lock-in amplifier were connected in series with calibrated Silicon and Germanium photodetectors to improve the signal-to-noise ratio for measurements. Higher sensitivity settings were used with a longer time delay between measurement points for the sub-band gap region. All EQE spectra were measured under zero voltage bias condition.

Photothermal Deflection Spectroscopy(PDS): PDS measurements were carried out with a standard setup consist of 1 kW Xe arc lamp and a 1/4 m grating monochromator (Oriel) as the tunable light source. The pump beam was modulated at 13 Hz by a mechanical chopper before irradiating on the sample. Perfluorohexane was used as the deflection fluid. A Uniphase HeNe laser was directed parallel to polymer sample surface as the probe laser. A quadrant cell (United Detector Technology) was used as the position sensor for monitoring the photothermal deflection signal of the probe beam. The output of the detector was fed into a lock-in amplifier (Stanford Research, Model SR830) for phase-sensitive measurements. All PDS spectra were normalized to the incident power of the pump beam. The experimental apparatus can be found in **Figure S7**.

Steady-state Photoluminescence (PL): The steady-state PL spectra were obtained with Ocean Optics USB2000 spectrometer. Different D-A weight ratio precursor solutions were

spin-coated and formed thin film on quartz. The excitation laser was used and the detector was located in front of films to acquire the PL signals. To compare those PL spectra of different D-A weight ratios, all the measurements were carried out with the fixed setup, including in the excitation source, detector and sample holder.

Atomic-force microscopy (AFM) surface morphology measurements: The samples were prepared by the same method as OPV devices, but without the top electrode. AFM images were scanned by Veeco diMultimodeV with NanoscopeV controller. The E-scanner with Appnano ACTA silicon probe scanned in tapping mode provided information of height and phase within a size of 2 micrometers.

Supporting Information

Supporting Information is available from the Wiley Online Library or from the author.

Acknowledgements

Support for this work under the Research Grant Council of Hong Kong under Grants #HKBU211913, #HKBU211412, and the Research Committee of HKBU under RC-ICRS/15-16/4A-SSK are is gratefully acknowledged.

Received: ((will be filled in by the editorial staff))

Revised: ((will be filled in by the editorial staff))

Published online: ((will be filled in by the editorial staff))

[1] H. Kang, G. Kim, J. Kim, S. Kwon, H. Kim, K. Lee, Adv. Mater. **2016**, *28*, 7821.
Bulk-Heterojunction Organic Solar Cells Five Core Technologies for Their Commercialization
[2] R. Steima, T. Ameri, P. Schilinskya, C. Waldaufc, G. Dennlerd, M. Scharberb, C. J. Brabece, *Solar Energy Materials and Solar Cells*. **2011**, *95*, 3256
Organic photovoltaics for low light applications
[3] H. K. H. Lee, Z. Li, J. Durrant, W. C. Tsoi, *Appl. Phys. Lett.* **2016**, *108*, 253301.
Is organic photovoltaics promising for indoor applications?
[4] A. J. Heeger, Adv. Mater. **2014**, *26*, 10
25th Anniversary Article: Bulk Heterojunction Solar Cells: Understanding the Mechanism of Operation.
[5] J. S. Moon , J. K. Lee , S. N. Cho , J. Y. Byun , A. J. Heeger, *Nano Lett.* **2009**, *9*, 230.
"Columnlike" Structure of the Cross-Sectional Morphology of Bulk Heterojunction Materials
[6] J. K. J. van Duren, X. Yang, J. Loos, C. W. T. Bulle-Lieuwma, A. B. Sieval, J. C. Hummelen, R. A. J. Janssen, *Adv. Funct. Mater*. **2004**, *14*, 425.
Relating the Morphology of Poly(p-phenylene vinylene)/Methanofullerene Blends to Solar-Cell Performance
[7] G. Li, V. Shrotriya, Y. Yao, Y. Yang, *J. Appl. Phys*. **2005**, *98*, 043704.
Investigation of annealing effects and film thickness dependence of polymer solar cells based on poly(3-hexylthiophene)
[8] G. Li, Y. Yao, H. Yang, V. Shrotriya, G. Yang, Y. Yang, *Adv. Funct. Mater*. **2007**, *17*, 1636.
"Solvent Annealing" Effect in Polymer Solar Cells Based on Poly(3-hexylthiophene) and Methanofullerenes
[9] J. K. Lee, W. L. Ma, C. J. Brabec, J. Yuen, J. S. Moon, J. Y. Kim, K. Lee, G. C. Bazan, A. J. Heeger, *J. Am. Chem. Soc*. **2008**, *130*, 3619.
Processing Additives for Improved Efficiency from Bulk Heterojunction Solar Cells

[10] H. Jhuo, S. Liao, Y. Li, P. Yeh, S. Chen, W. Wu, C. Su, J. Lee, N. Yamada, U. Jeng, *Adv. Funct. Mater*. **2016**, *26*, 3094.
The Novel Additive 1-Naphthalenethiol Opens a New Processing Route to Efficiency-Enhanced Polymer Solar Cells
[11] Z. Xiao, Y. Yuan, B. Yang, J. VanDerslice, J. Chen, O. Dyck, G. Duscher, J. Huang, Adv. Mater. **2014**, *26*, 3068.
Universal Formation of Compositionally Graded Bulk Heterojunction for Efficiency Enhancement in Organic Photovoltaics
[12] Y. Liang, Z. Xu, J. Xia, S. Tsai, Y. Wu, G. Li, C. Ray, L. Yu, *Adv. Mater*. **2010**, 22, E135.
For the Bright Future-Bulk Heterojunction Polymer Solar Cells with Power Conversion Efficiency of 7.4%
[13] M. Campoy-Quiles, T. Ferenczi, T. Agostinelli, P. Etchegoin, Y. Kim, T. Anthopoulos, P. Stavrinou, D. Bradley, J. Nelson, Nature Materials, **2008**, *7*, 158.
Morphology evolution via self-organization and lateral and vertical diffusion in polymer:fullerene solar cell blends.
[14] R. Pacios, J. Nelson, D. D. C. Bradley, C. J. Brabec, *Appl. Phys. Lett*. **2003**, *83*, 4764.
Composition dependence of electron and hole transport in polyfluorene:[6,6]-phenyl C61-butyric acid methyl ester blend films
[15] D. Chirvase, J. Parisi, J. Hummelen, V. Dyakonov, Nanotechnology **2004**, *15*, 1317.
Influence of nanomorphology on the photovoltaic action of polymer–fullerene composites
[16] V. D. Mihailetchi, L. J. A. Koster, P. W. M. Blom, C. Melzer, B. de Boer, J. K. J. van Duren, R. A. J. Janssen, *Adv. Funct. Mater.* **2005**, *15*, 795.
Compositional Dependence of the Performance of Poly(p-phenylene vinylene) : Methanofullerene Bulk-Heterojunction Solar Cells
[17] C. Müller, T. A. M. Ferenczi, M. Campoy-Quiles, J. M. Frost, D. D. C. Bradley, P. Smith, N. Stingelin-Stutzmann, J. Nelson, *Adv. Mater.* **2008**, *20*, 3510.
Binary Organic Photovoltaic Blends: A Simple Rationale for Optimum Compositions
[18] V. Pranculis, A. Ruseckas, D. A. Vithanage, G. J. Hedley, I. D. W. Samuel, V. Gulbinas, *J. Phys. Chem.* **2016**, *120*, 9588.
Influence of Blend Ratio and Processing Additive on Free Carrier Yield and Mobility in PTB7:PC71BM Photovoltaic Solar Cells
[19] J. K. J. van Duren, X. Yang, J. Loos, C. W. T. Bulle-Lieuwma, A. B. Sieval, J. C. Hummelen, R. A. J. Janssen, *Adv. Funct. Mater*. **2004**, *14*, 425.
Relating the Morphology of Poly(p-phenylene vinylene)/Methanofullerene Blends to Solar-Cell Performance
[20] R. Lin, M. Wright, B. Puthen-Veettil, X. Wen, M. J. Y. Tayebjee, A. Uddin, *Phys. Status Solidi A*, **2015**, *212*, 1931.
Effects of blend composition on the morphology of Si-PCPDTBT:PC71 BM bulk heterojunction organic solar cells
[21] X. Guo, M. Zhang, J. Tan, S. Zhang, L. Huo, W. Hu, Y. Li, J. Hou, *Adv. Mater.*, **2012**, *24*, 6536 .
Influence of D/A Ratio on Photovoltaic Performance of a Highly Efficient Polymer Solar Cell System
[22] K. Vakhshouri, D. R. Kozub, C. Wang, A. Salleo, E. Gomez, *Phys. Rev. Lett*. **2012**, *108.2*, 026601
Effect of miscibility and percolation on electron transport in amorphous poly (3-hexylthiophene)/phenyl-C61-butyric acid methyl ester blends
[23] J. A. Bartelt, Z. M. Beiley, E. T. Hoke, W. R. Mateker, J. D. Douglas, B. A. Collins, J. R. Tumbleston, K. R. Graham, A. Amassian, H. Ade, J. M. J. Fréchet, M. F. Toney, M. D. McGehee, *Adv. Energy Mater.* **2012**, *3*, 364.

The Importance of Fullerene Percolation in the Mixed Regions of Polymer–Fullerene Bulk Heterojunction Solar Cells
[24] S. Nho, G. Baek, S. Park, B. R. Lee, M. J. Cha, D. C. Lim, J. H. Seo, S.-H. Oh, M. H. Song, S. Cho, *Energy Environ. Sci.* **2016**, *9*, 240.
Highly efficient inverted bulk-heterojunction solar cells with a gradiently-doped ZnO layer
[25] M. A. Lampert , P. Mark , *Current Injection in Solids* , Academic ,New York **1970**.
[26] P. N. Murgatroyd , *J. Phys. D.*, **1970** , *3*, 151.
Theory of space-charge-limited current enhanced by Frenkel effect
[27] A. Rose, *Concepts in photoconductivity and allied problems*, Interscience Publishers, New York, **1963**
[28] V. D. Mihailetchi, J. K. J. van Duren, P. W. M. Blom, J. C. Hummelen, R. A. J. Janssen, J. M. Kroon, M. T. Rispens, W. J. H. Verhees, M. M. Wienk, *Adv. Funct. Mater.* **2003**, *13*, 43.
Electron transport in a methanofullerene
[29] H. K. H. Lee, K. K. H. Chan, S. K. So, *Org. Electron.* **2012**, *13*, 541.
Role of electron blocking and trapping layers in transport characterization of a photovoltaic polymer poly(3-hexylthiophene)
[30] C. H. Y. Ho, Q. Dong, H. Yin, W. W. K. Leung, Q. Yang, H. K. H. Lee, S. W. Tsang, S. K. So, *Adv. Mat. Interfaces.* **2015**, *2*, 1500166.
Impact of Solvent Additive on Carrier Transport in Polymer: Fullerene Bulk Heterojunction Photovoltaic Cells
[31] H. Bässler, *Phys. Status Solidi B.* **1993**, *175*, 15.
Charge Transport in Disordered Organic Photoconductors a Monte Carlo Simulation Study
[32] W. Y. Sit, S. H. Cheung, C. Y. H. Chan, K. K. Tsung, S. W. Tsang, S. K. So, *Adv. Electron. Mater.* **2016**, *2*, 1500273.
Probing Bulk Transport, Interfacial Disorders, and Molecular Orientations of Amorphous Semiconductors in a Thin-Film Transistor Configuration
[33] N. M. Amer, W. B. Jackson, *Semiconductors and Semimetals*, **1984**, *21*, 83
Optical Properties of Defect States in a-Si: H
[34] L. Goris, A. Poruba, L. Hod'ákova, M. Vaněček, K. Haenen, M. Nesládek, P. Wagner, D. Vanderzande, L. De Schepper, J. Manca, *Appl. Phys. Lett.* **2006**, *88*, 052113
Observation of the subgap optical absorption in polymer-fullerene blend solar cells
[35] W. B. Jackson, N. M. Amer, A. C. Boccara, D. Fournier, *Appl. Opt.* **1981**, *20*, 1333.
Photothermal deflection spectroscopy and detection
[36] M. H. Chan, S. K. So, and K. W. Cheah, *J. Appl. Phys.* **1996**, *79*, 3273
Optical Absorption of Free Standing Porous Silicon Thin Films
[37] M. Kuik, J. Vandenbergh, L. Goris, E. Begemann, L. Lutsen, D. J. M. Vanderzande, J. V. Manca, P. W. M. Blom, *Appl. Phys. Lett.* **2011**, *99*, 183305.
Optical detection of deep electron traps in poly(p-phenylene vinylene) light-emitting diodes
[38] S. So, M. Chan, L. Leung, *Appl. Phys. A.* **1995**, *61*, 159.
Photothermal Deflection Spectroscopy of Polymer Material
[39] M. H. Brodsky, M. Cardona, J. J. Cuomo, *Phys. Rev. B*, **1977**, *16*, 3556.
Infrared and Raman spectra of the silicon-hydrogen bonds in amorphous silicon prepared by glow discharge and sputtering
[40] F. Urbach, *Phys. Rev.* **1953**, *92*, 1324.
The Long-Wavelength Edge of Photographic Sensitivity and of the Electronic Absorption of Solids
[41] I. Constantinou, T.-H. Lai, H.-Y. Hsu, S. H. Cheung, E. D. Klump, K. S. Schanze, S. K. So, F. So, *Adv. Electron. Mater.* **2015**, *1*, 1500167.
Effect of Thermal Annealing on Charge Transfer States and Charge Trapping in PCDTBT:PC70BM Solar Cells

[42] C. Nam, D. Su, C. Black, *Adv. Funct. Mater.* **2009**, *19*, 3552.
High-Performance Air-Processed Polymer–Fullerene Bulk Heterojunction Solar Cells
[43] M. M. Mandoc, F. B. Kooistra, J. C. Hummelen, B. de Boer, P. W. Blom, *App. Phys. Lett.* **2007**, *91*, 263505.
Effect of traps on the performance of bulk heterojunction organic solar cells
[44] H. Yan, J. G. Manion, M. Yuan, F. P. García de Arquer, G. R. McKeown, S. B. Beaupré, M. Leclerc, E. H. Sargent, D. S. Seferos, *Adv. Mater.* **2016**, *28*, 6491.
Increasing Polymer Solar Cell Fill Factor by Trap-Filling with F4-TCNQ at Parts Per Thousand Concentration
[45] J. Schafferhans, A. Baumann, A. Wagenpfahl, C. Deibel, V. Dyakonov, *Org. Electron.* **2010**, *11*, 1693.
Oxygen doping of P3HT:PCBM blends: Influence on trap states, charge carrier mobility and solar cell performance
[46] K. S. Nalwa, R. C. Mahadevapuram, S. Chaudhary, *App. Phys. Lett.* **2011**, *98*, 093306.
Growth rate dependent trap density in polythiophene-fullerene solar cells and its implications
[47] E. Buchaca-Domingo, K. Vandewal, Z. Fei, S. E. Watkins, F. H. Scholes, J. H. Bannock, J. C. de Mello, L. J. Richter, D. M. DeLongchamp, A. Amassian, M. Heeney, A. Salleo, N. Stingelin, *J. Am. Chem. Soc.* **2015**, *137*, 5256.
Direct Correlation of Charge Transfer Absorption with Molecular Donor:Acceptor Interfacial Area via Photothermal Deflection Spectroscopy
[48] F. Wooten, *Optical properties of solids*, Acad. Press, New York, **1972**
[49] J. Workman, L. Weyer, *Practical guide and spectral atlas for interpretive near-infrared spectroscopy*, CRC Press, Boca Raton, **2012**.
[50] L. Goris, K. Haenen, M. Nesládek, P. Wagner, D. Vanderzande, L. De Schepper, J. D'haen, L. Lutsen, J. Manca, *J. Mater. Sci.* **2005**, *40*, 1413.
Absorption phenomena in organic thin films for solar cell applications investigated by photothermal deflection spectroscopy
[51] K. R. Graham, C. Cabanetos, J. P. Jahnke, M. N. Idso, A. El Labban, G. O. Ngongang Ndjawa, T. Heumueller, K. Vandewal, A. Salleo, B. F. Chmelka, A. Amassian, P. M. Beaujuge, M. D. McGehee, *J. Am. Chem. Soc.* **2014**, *136*, 9608.
Importance of the Donor:Fullerene Intermolecular Arrangement for High-Efficiency Organic Photovoltaics
[52] V. Gupta, V. Bharti, M. Kumar, S. Chand, A. J. Heeger, *Adv. Mater.* **2015**, *27*, 4398.
Polymer–Polymer Förster Resonance Energy Transfer Significantly Boosts the Power Conversion Efficiency of Bulk-Heterojunction Solar Cells
[53] B. A. Collins, Z. Li, J. R. Tumbleston, E. Gann, C. R. McNeill, H. Ade, *Adv. Energy Mater.* **2013**, *3*, 65.
Absolute Measurement of Domain Composition and Nanoscale Size Distribution Explains Performance in PTB7:PC71BM Solar Cells

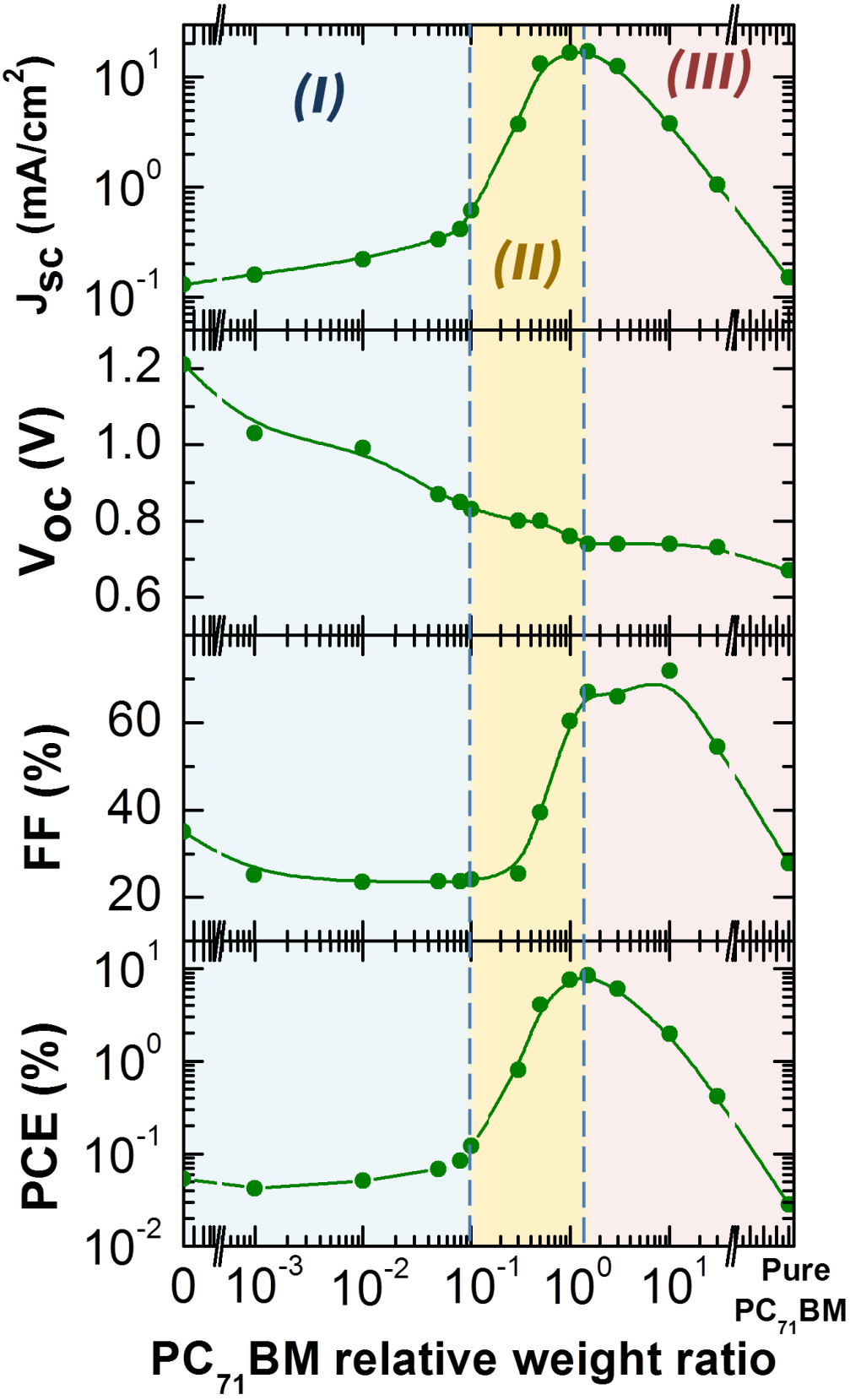

Figure 1. Summary plots of PTB7:$PC_{71}BM$ OPV cells performance at different donor : acceptor weight ratio.

Donor-acceptor weight ratio	J_{sc} [mA cm^{-2}]	V_{oc} [V]	FF [%]	PCE [%]
1 : 0	0.13	1.21	35	0.054
1 : 0.001	0.16	1.03	25	0.042
1 : 0.01	0.22	0.99	23	0.051
1 : 0.05	0.33	0.87	24	0.068
1 : 0.08	0.41	0.85	24	0.083
1 : 0.1	0.61	0.83	24	0.122
1 : 0.3	3.71	0.80	25	0.8
1 : 0.5	13.19	0.80	39	4.1
1 : 1	16.58	0.76	60	7.6
1 : 1.5	16.90	0.74	67	8.4
1 : 3	12.48	0.74	66	6.1
1 : 10	3.77	0.74	72	2.0
1 : 30	1.04	0.73	55	0.4
0 : 1	0.15	0.67	28	0.029

Table 1. Summary of the performances of OPV cells using PTB7:$PC_{71}BM$ as active materials for different donor:acceptor weight ratio.

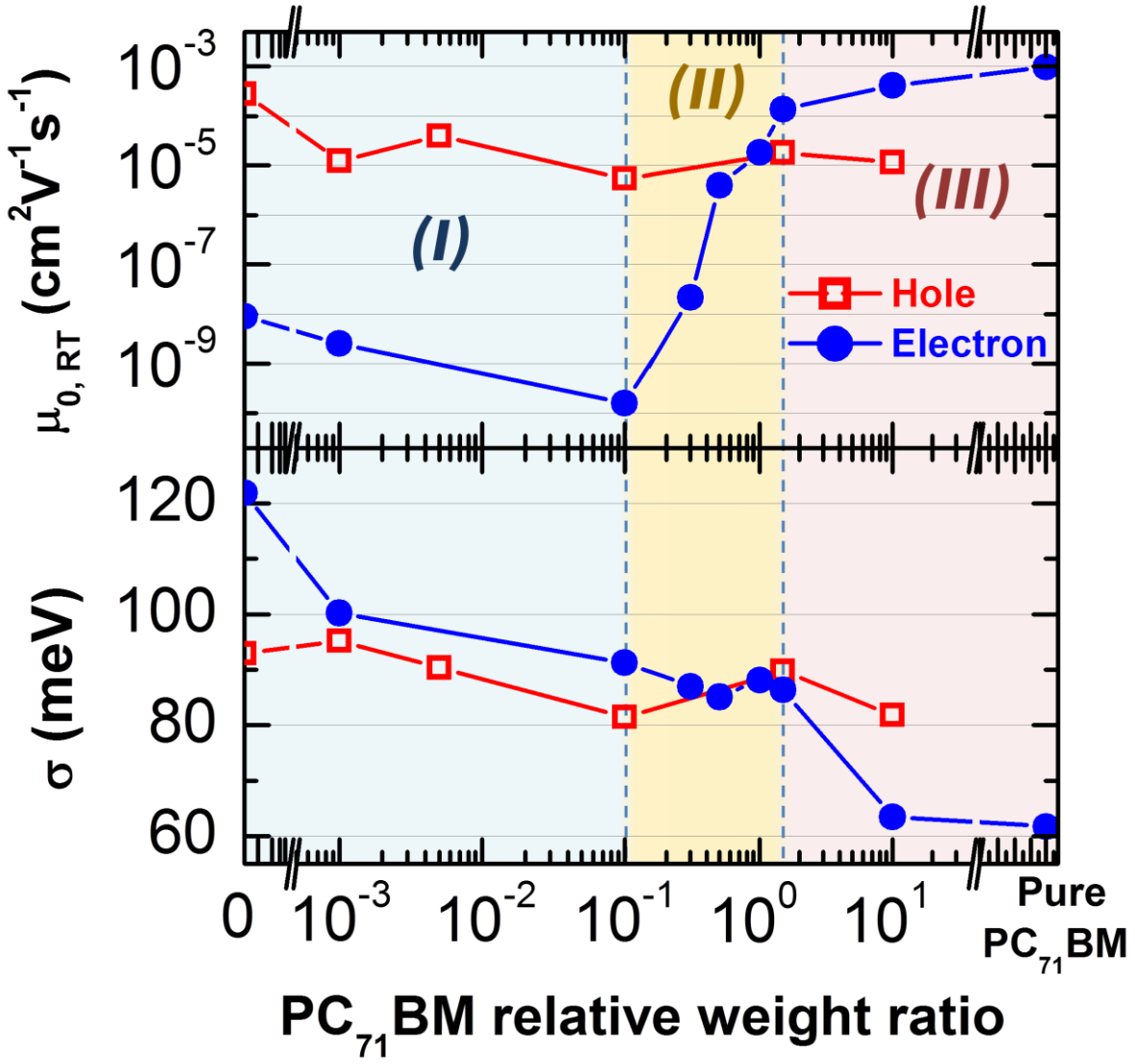

Figure 2. Summary plots for transport parameters of BHJ films at room temperature (a) Zero-field mobilities, (b) Energetic disorders

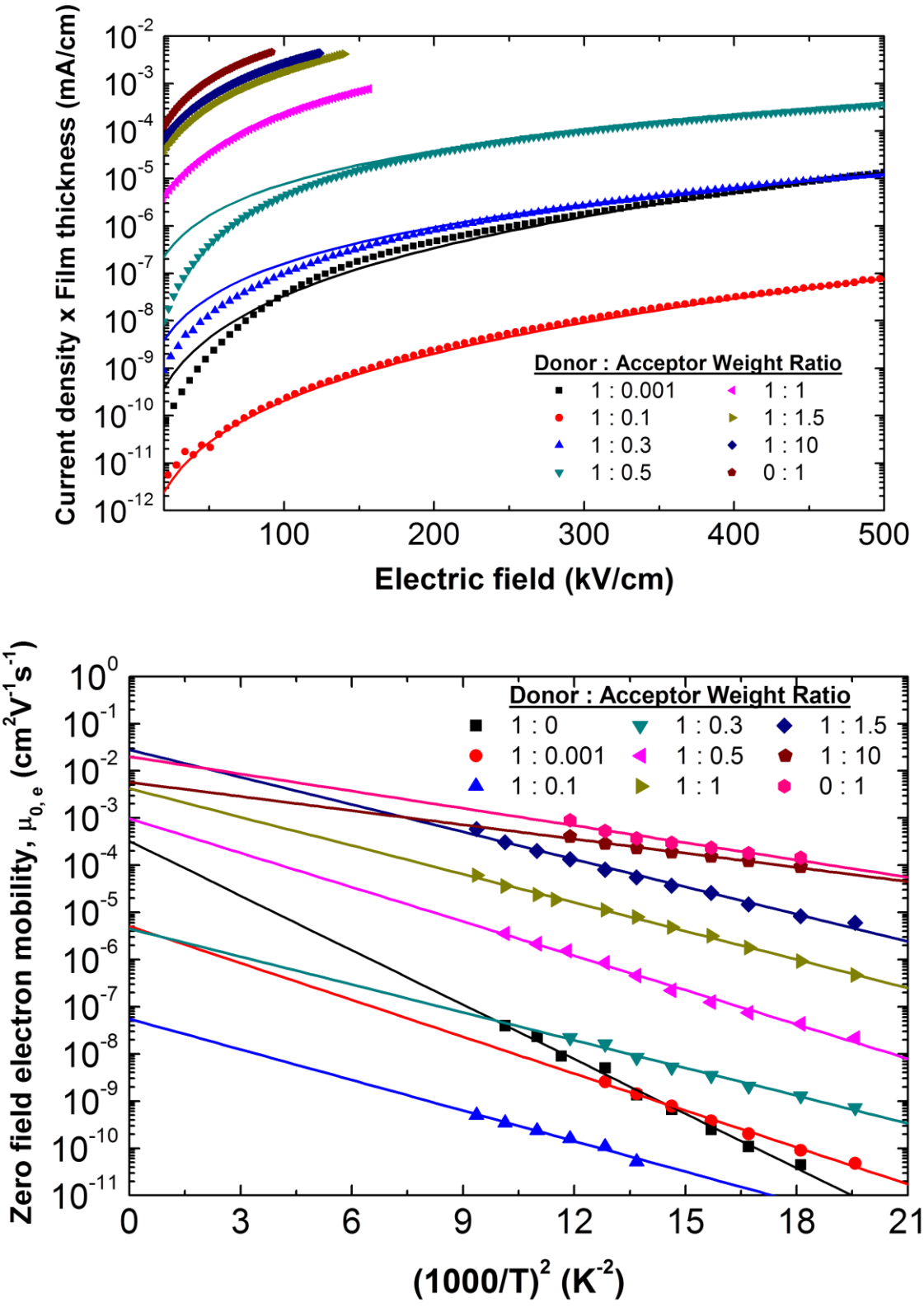

Figure 3. (a) J-V characteristics of PTB7:$PC_{71}BM$ electron-only device with different donor : acceptor weight ratio at room temperature in a semi-log plot. The solid lines represent the best fit to SCLC model with traps. (b) Zero-field electron mobility versus $1/T^2$. The solid lines are best linear fits to the experimental data.

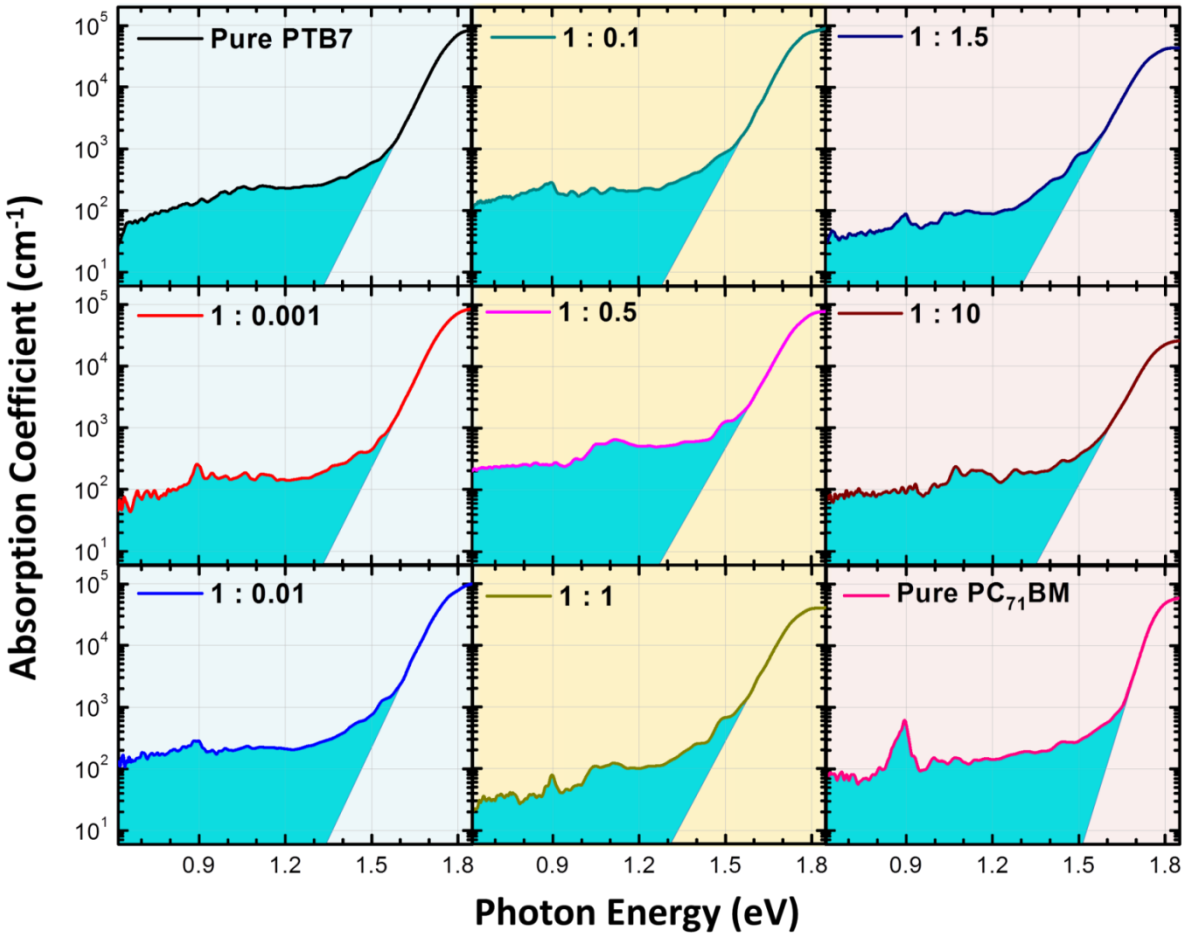

Figure 4. Photothermal deflection spectroscopy spectra with different D-A weight ratios. The region under curve shaded in pale blue indicates the trap states.

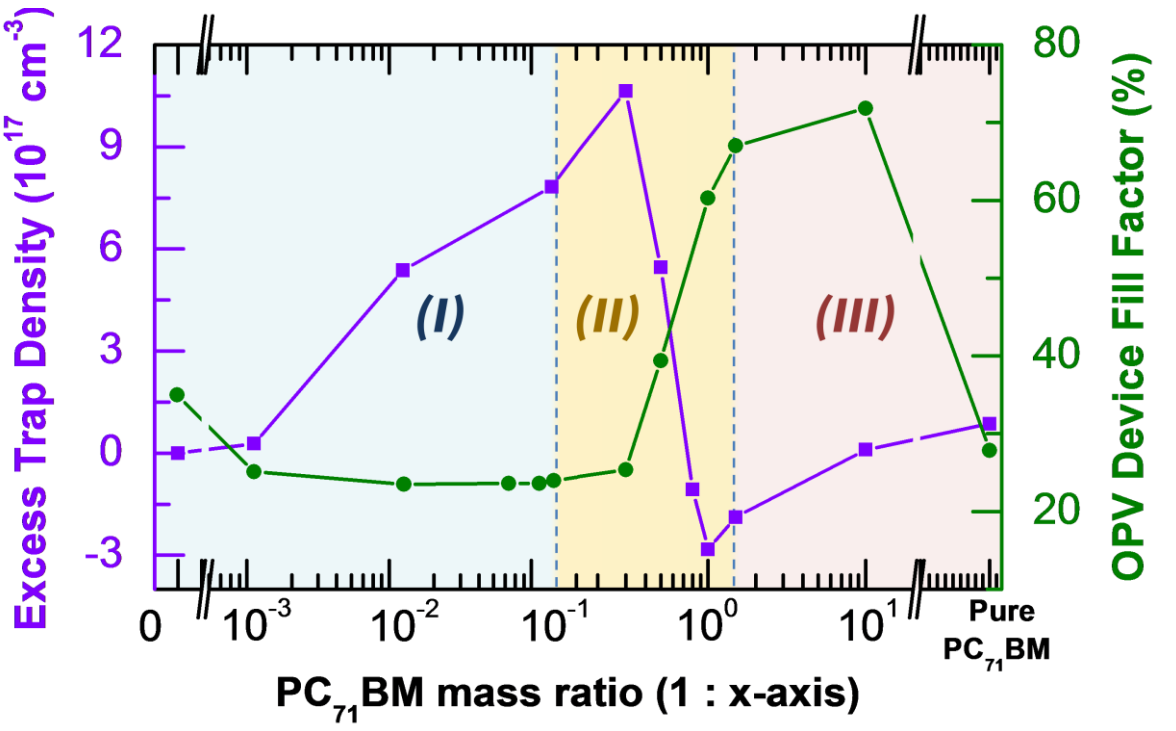

Figure 5. Correlation between OPV device FF and calculated trap density from PDS signal using optical sum rule

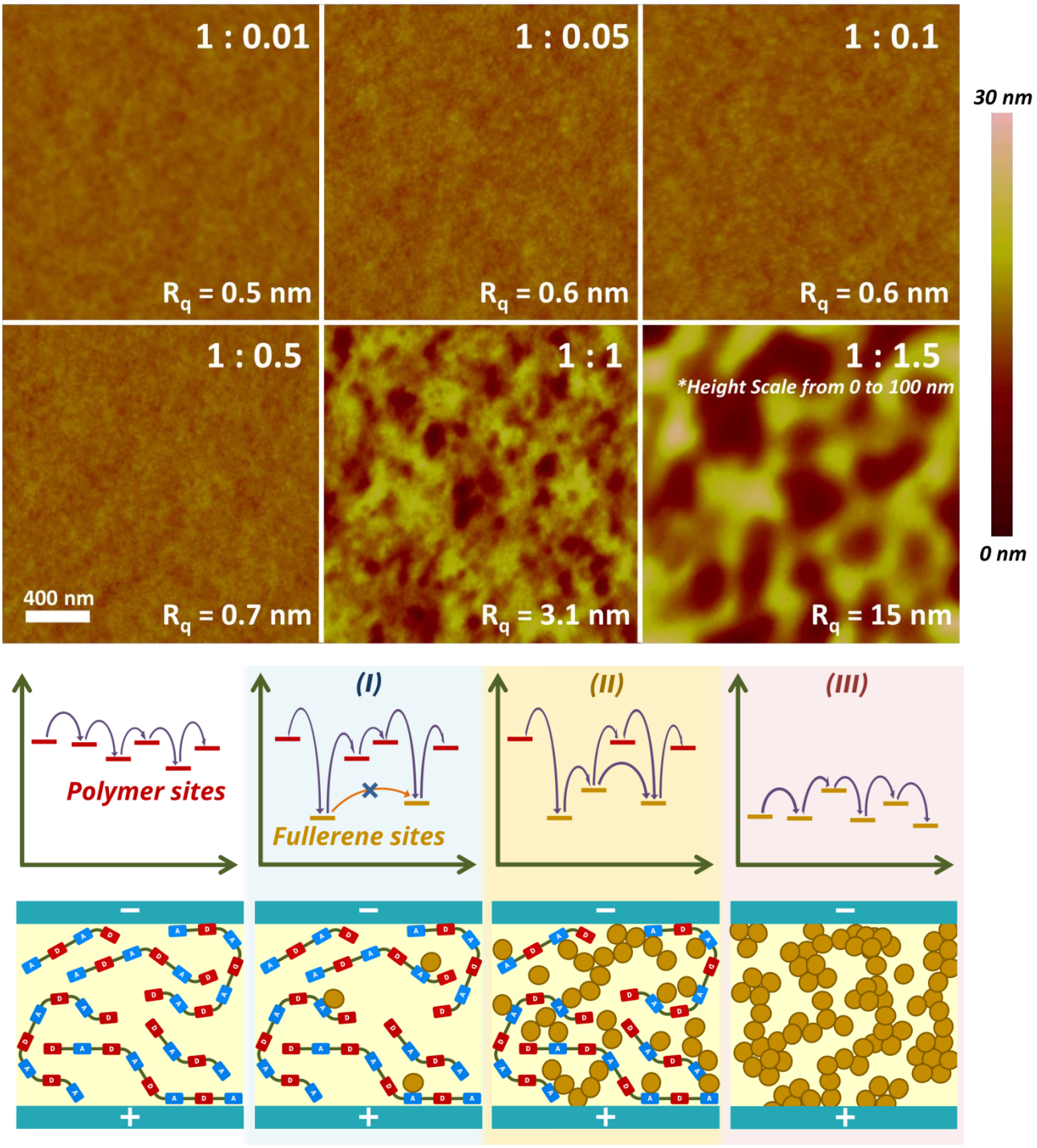

Figure 6. (a-f) AFM images of BHJ films at different D-A ratio in height mode (g) Schematic diagrams show the percolation of fullerene domains: Different hopping regimes in a disordered host–guest system: Hopping via polymer sites; hopping via polymer sites in the presence of a small amount of fullerene sites (trap-limited transport); hopping via both host and guest sites; hopping via guest sites.

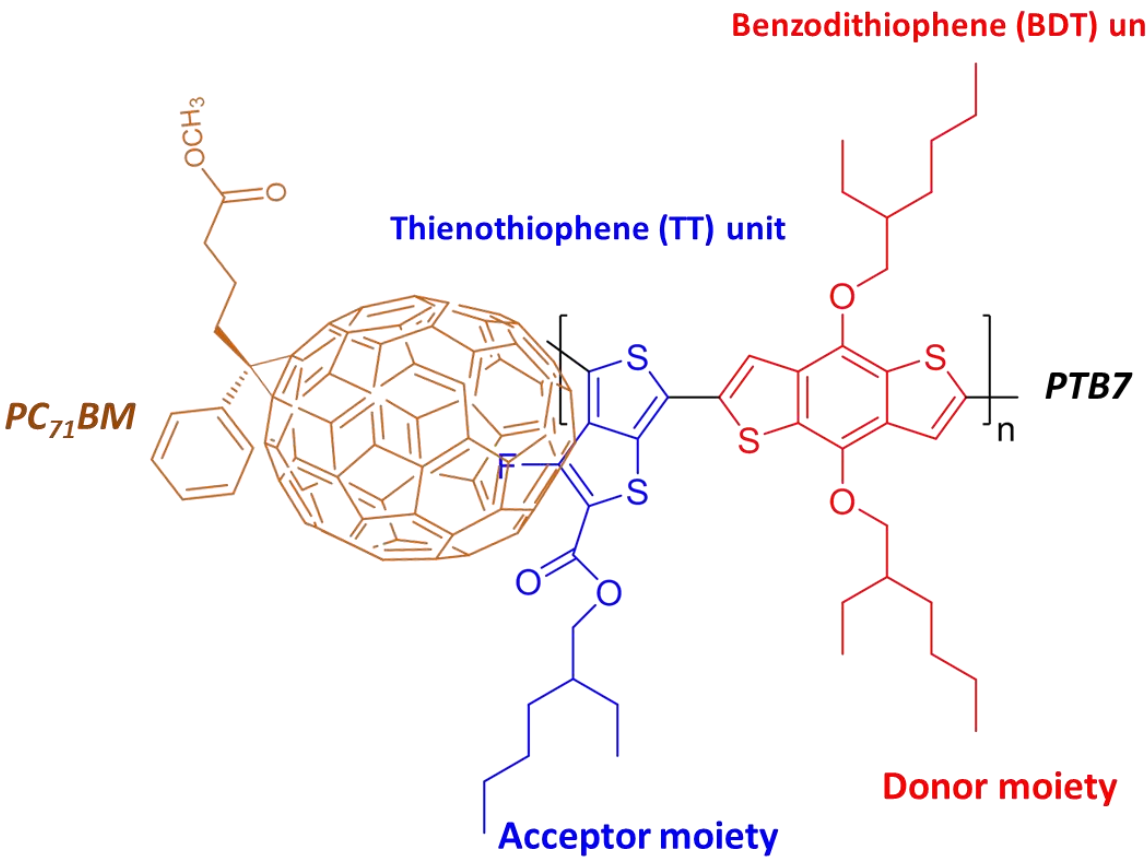

Figure 7. A simplified model illustrating the interaction between $PC_{71}BM$ and the PTB7. As shown in the picture, the fullerene prefers docking with the acceptor moiety (TT unit) of PTB7, due to the steric effect from the long side chain in the donor moiety (BDT unit) of PTB7.

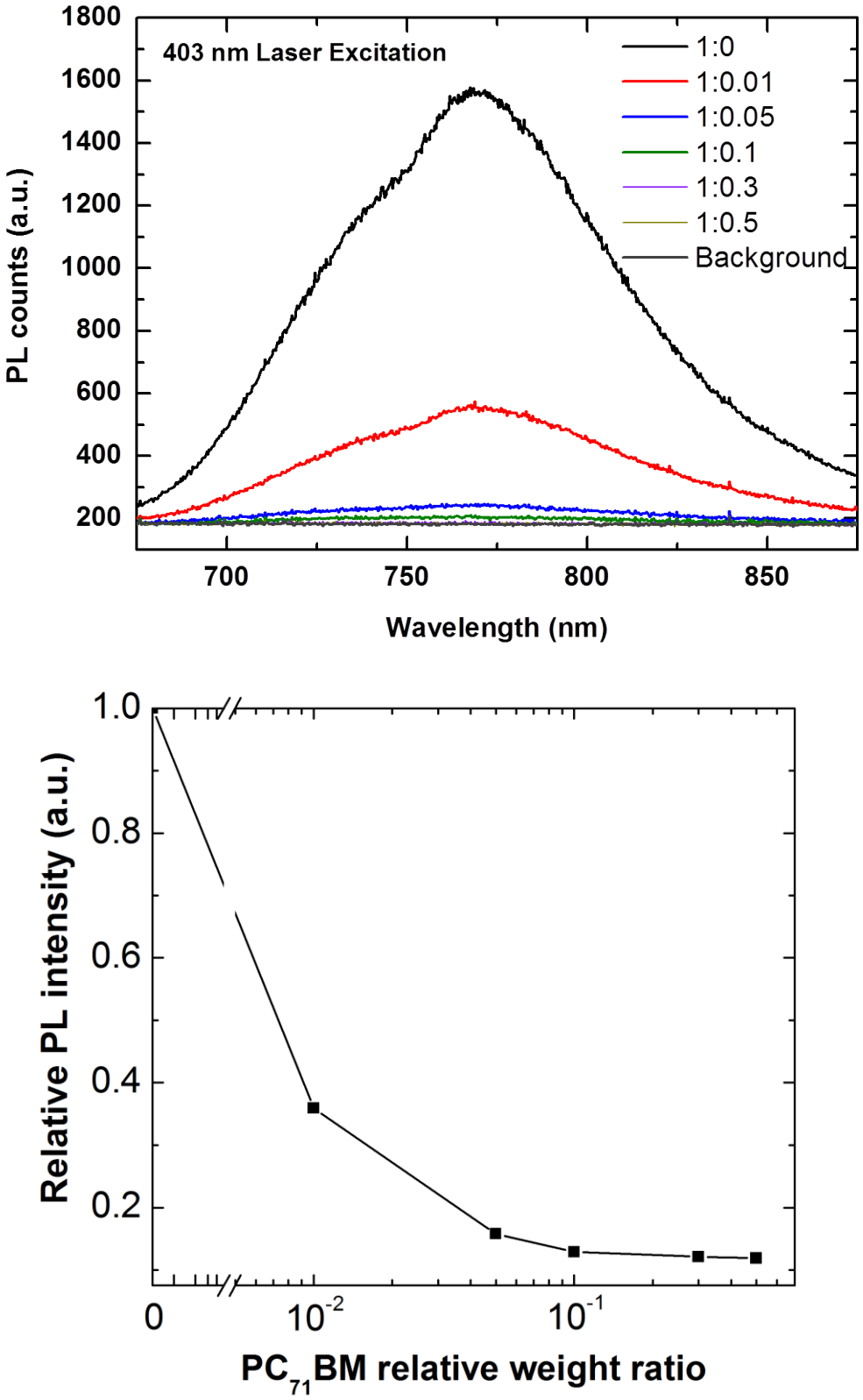

Figure 8. (a) Steady-state photoluminescence (PL) spectrum of BHJ films at different D-A weight ratio, 403 nm laser was used to excite the film. (b) Normalized intensity value comparison of PL spectrum at 775 nm .

Table of content

Ultra-low dosages of fullerene in bulk heterojunction is used to reveal the early stage electronic donor-acceptor interactions. Before percolation occurs, fullerene dock with polmer backbone and act as electron traps. It increases electron trap density and lowers the electron mobility. The fill factors of the corresponding photovolatic devices are found to anti-correlate with the trap density.

Keyword: bulk heterojunction, traps, photothermal deflection spectroscopy, carrier transport, photovoltaic

Carr Hoi Yi Ho, Sin Hang Cheung, Ho Wa Li, Ka Lok Chiu, Yuanhang Cheng, Hang Yin, Mau Hing Chan, Franky So, Sai Wing Tsang, Shu Kong So

Using Ultra-Low Dosages of Electron Acceptor to Reveal Electronic Interactions Between Donors and Acceptors

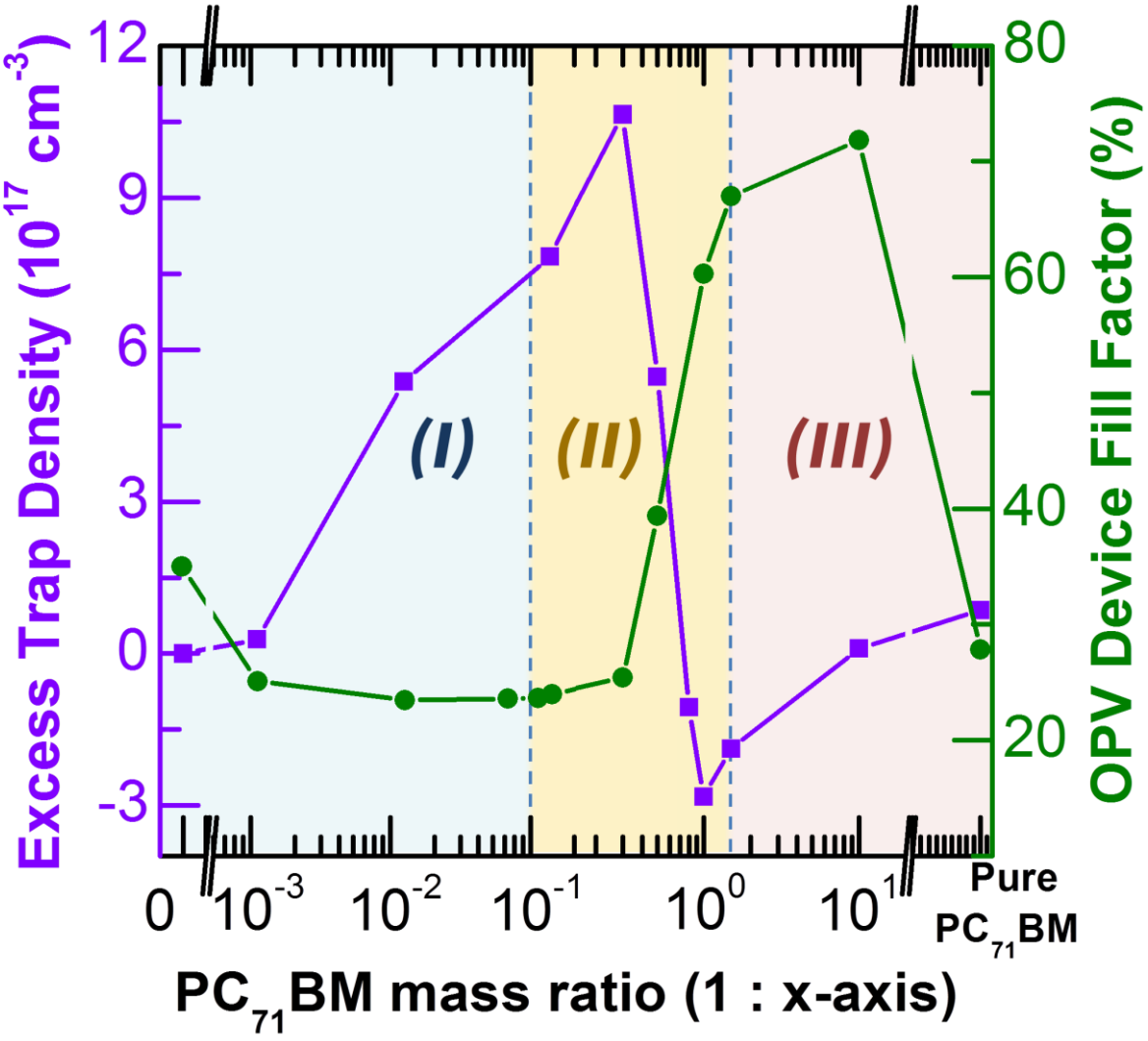

Copyright WILEY-VCH Verlag GmbH & Co. KGaA, 69469 Weinheim, Germany, 2013.

Supporting Information

Title: Using Ultra-Low Dosages of Electron Acceptor to Reveal Electronic Interactions Between Donors and Acceptors

Carr Hoi Yi Ho, Sin Hang Cheung, Ho Wa Li, Ka Lok Chiu, Yuanhang Cheng, Hang Yin, Mau Hing Chan, Franky So, Sai Wing Tsang, Shu Kong So

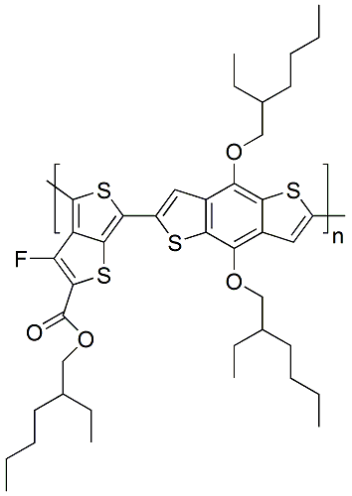

(a)

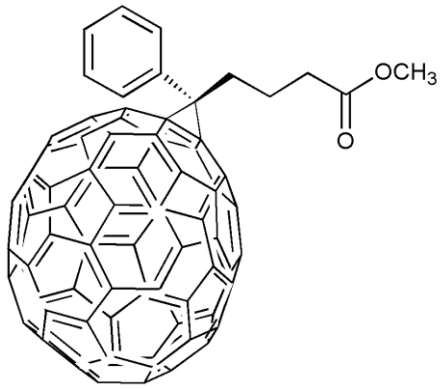

(b)

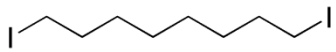

(c)

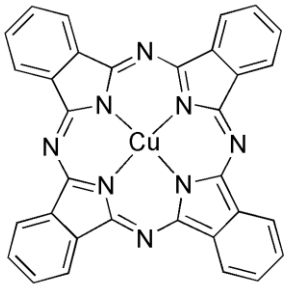

(d)

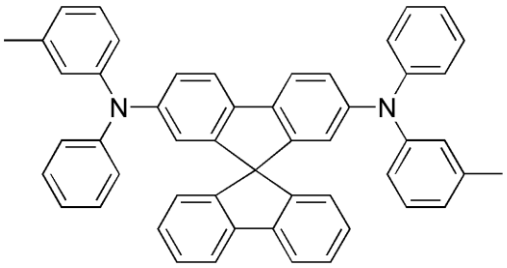

(e)

Figure S1. Chemical structures of (a) PTB7, (b) $PC_{71}BM$, (c) DIO (d) copper(II) phthalocyanine (CuPc), and (e) N,N'-bis(3-methylphenyl)-N,N'-bis(phenyl)-9,9-spirobifluorene (Spiro-TPD).

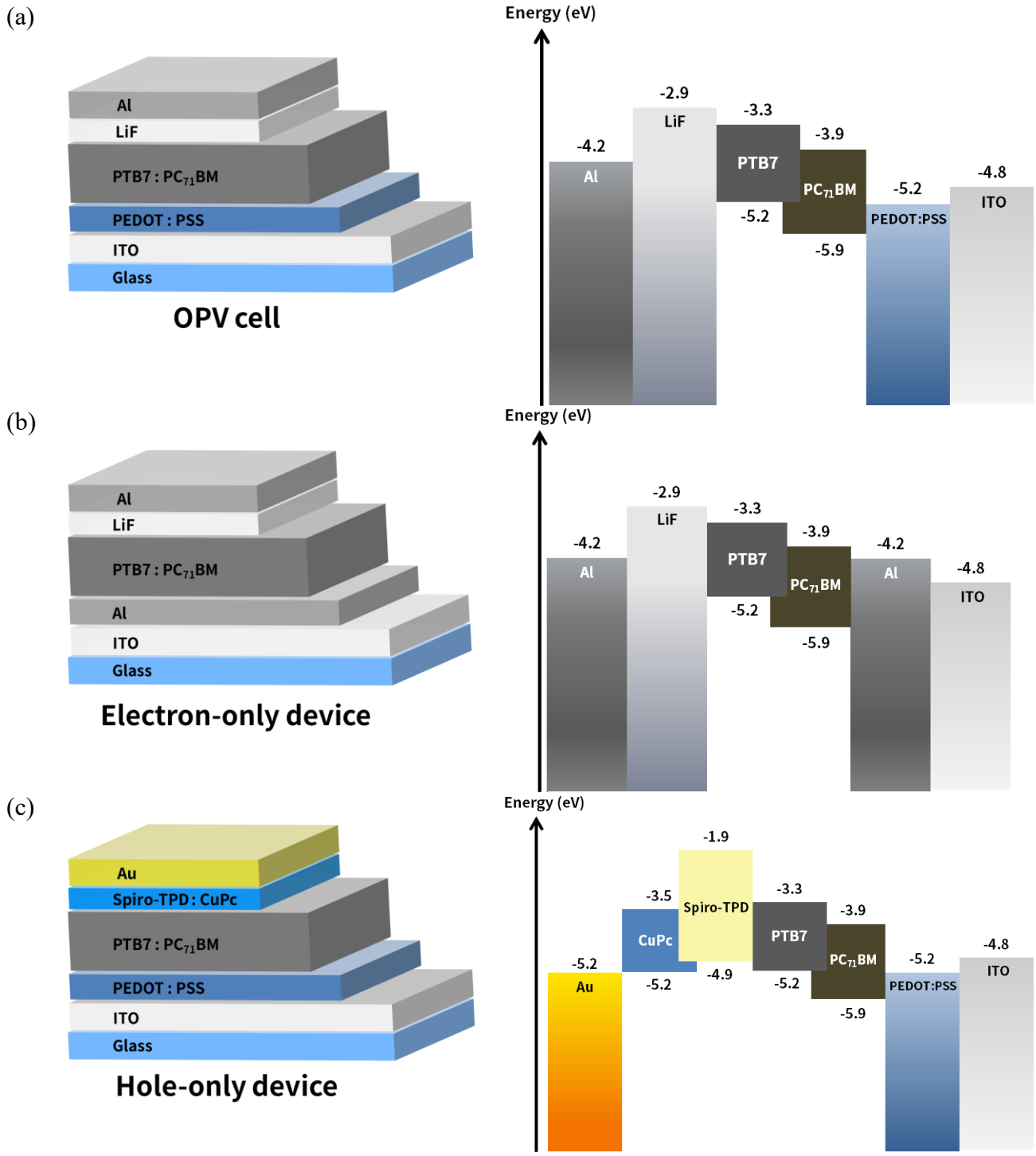

Figure S2. Device structures of BHJ of PTB7:$PC_{71}BM$. (a) OPV cell, (b) electron-only, and (c) hole-only device for carrier transport evaluation, and their schematic energy levels. In (b), the interlayer of spiro-TPD:CuPc act as an electron-blocking and trapping layer. In (c), a thin layer of CB is spin-coated on the bottom Al electrode for better wetting.

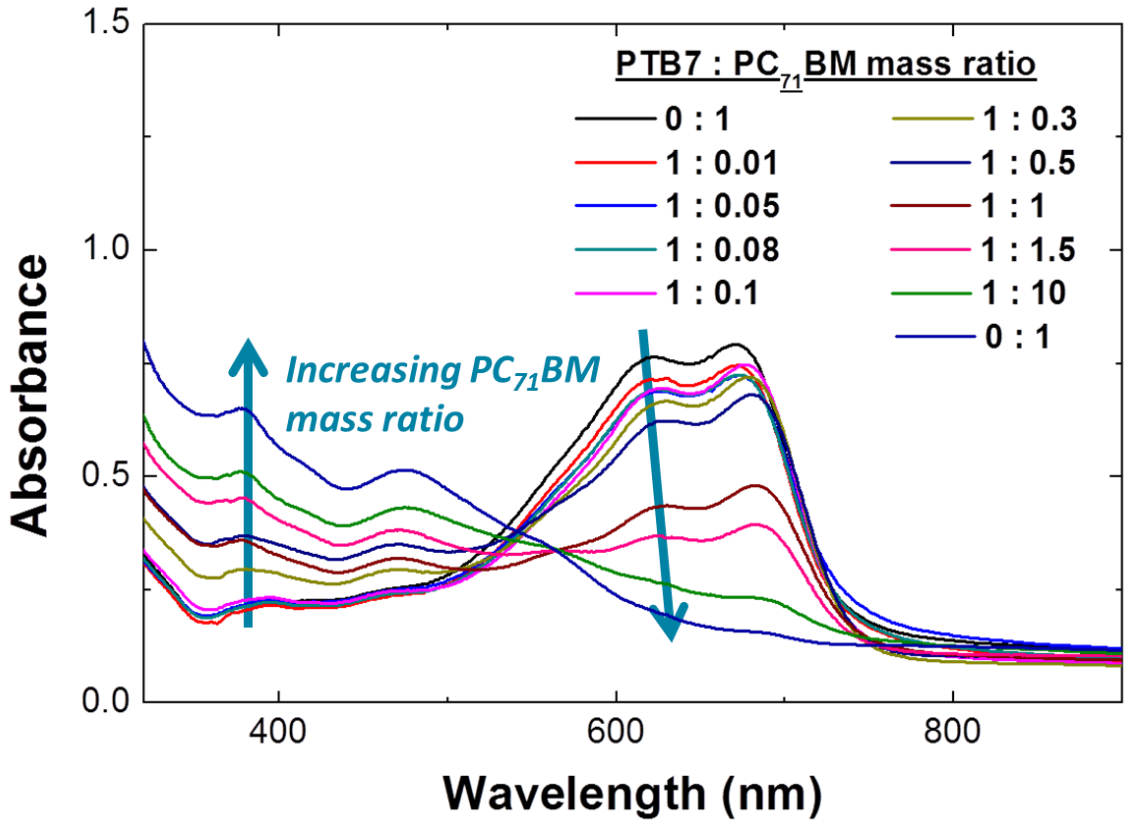

Figure S3. Ultraviolet-visible absorption spectra different D-A ratio, the film thickness were kept around 100nm

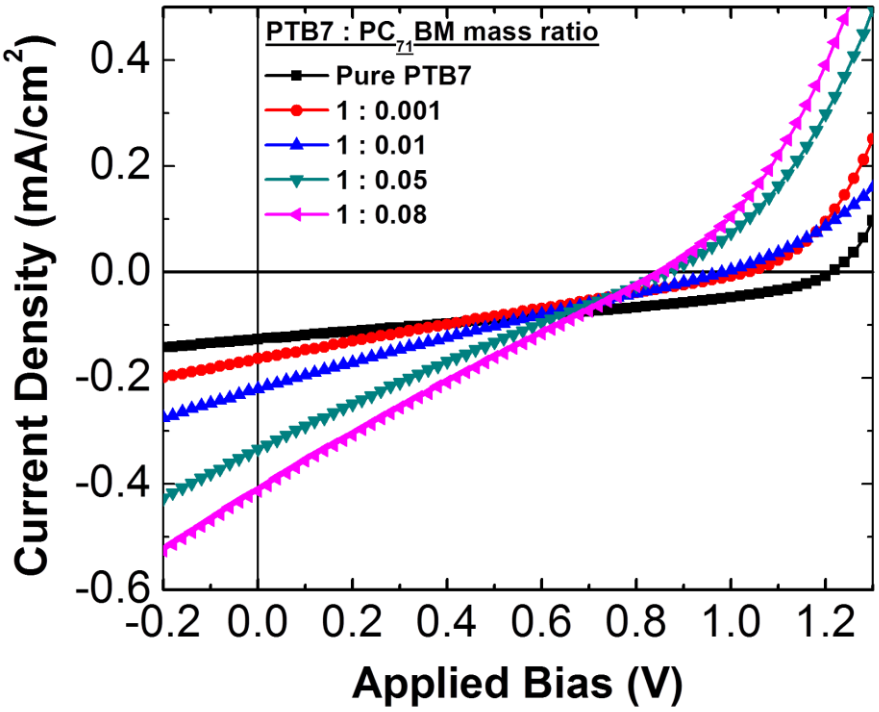
PTB7 : PC71BM mass ratio
Pure PTB7
1 : 0.001
1 : 0.01
1 : 0.05
1 : 0.08
Current Density (mA/cm2)
Applied Bias (V)
0.4
0.2
0.0
-0.2
-0.4
-0.6
-0.2
0.0
0.2
0.4
0.6
0.8
1.0
1.2

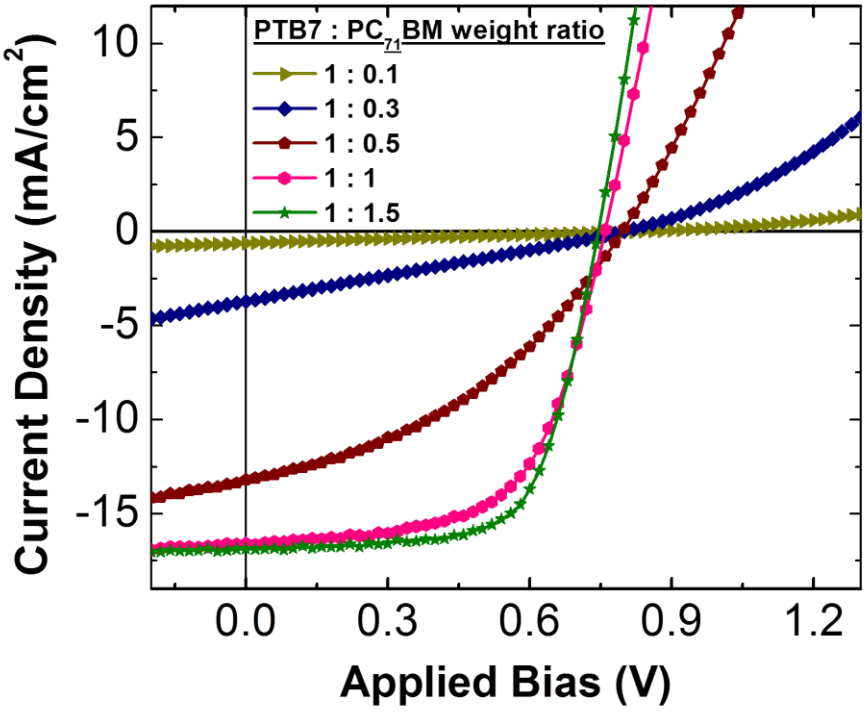
PTB7 : PC71BM weight ratio
1 : 0.1
1 : 0.3
1 : 0.5
1 : 1
1 : 1.5
Current Density (mA/cm2)
Applied Bias (V)
10
5
0
-5
-10
-15
0.0
0.3
0.6
0.9
1.2

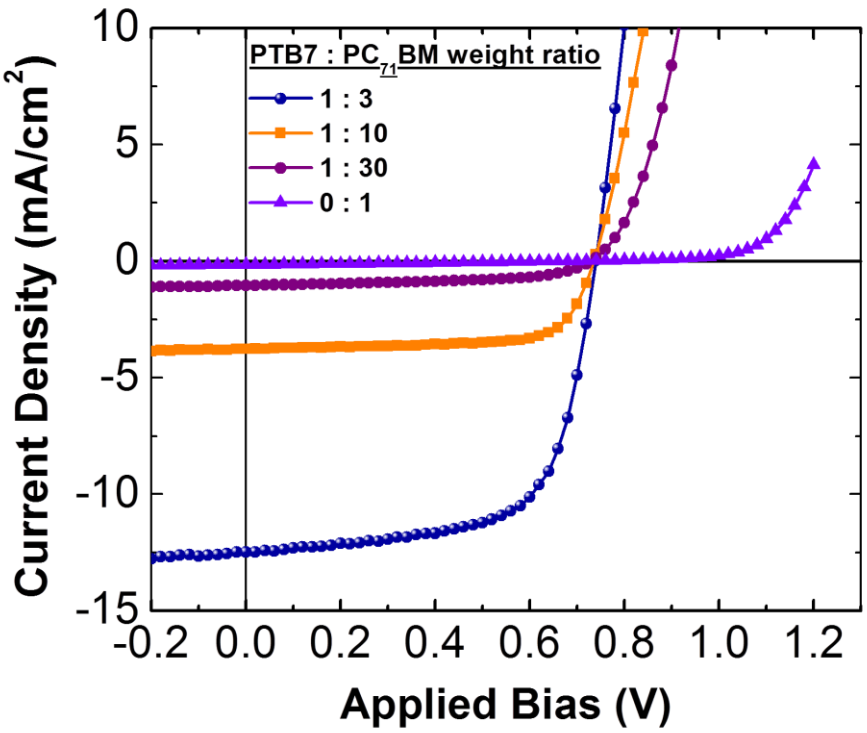

Figure S4. Current-voltage characteristics of OPV devices at different D-A ratios.

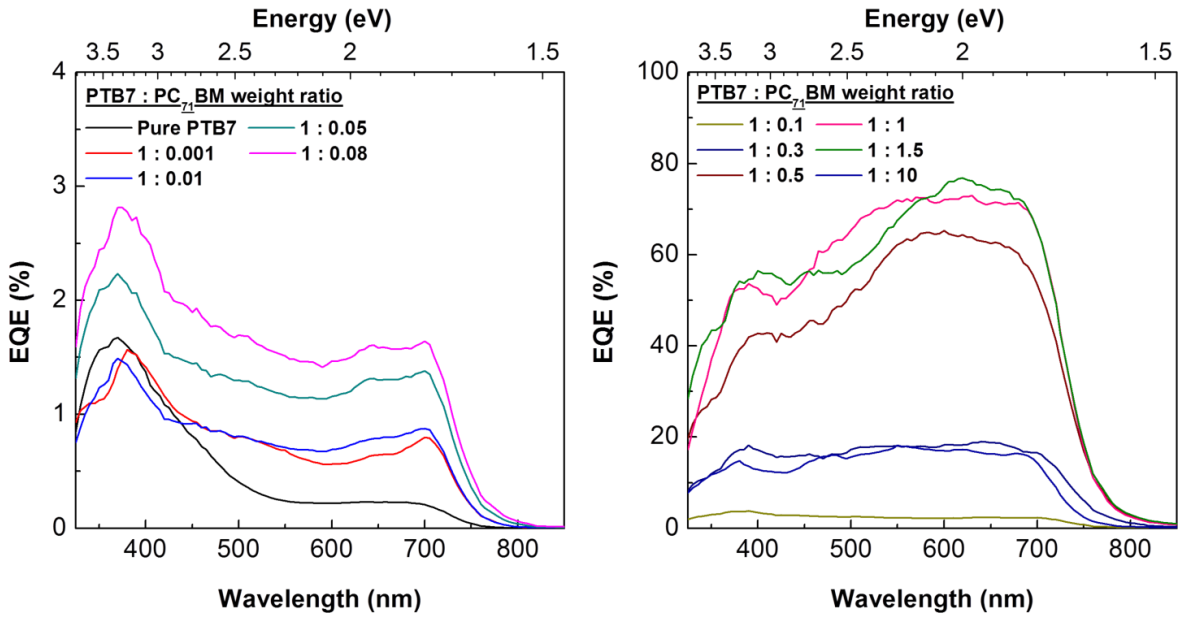

Figure S5. External quantum efficiency curves of OPV devices at different D-A weight ratios.

Donor-Acceptor weight ratio	Electron mobility ($cm^2V^{-1}s^{-1}$)	Energetic Disorder (meV)
1 : 0	9.0×10^{-9}	122
1 : 0.001	2.6×10^{-9}	100
1 : 0.1	1.1×10^{-10}	91
1 : 0.3	2.2×10^{-8}	87
1 : 0.5	4.0×10^{-6}	85
1 : 1	1.9×10^{-5}	88
1 : 1.5	2.2×10^{-4}	81
1 : 10	4.1×10^{-4}	63
0 : 1	9.7×10^{-4}	62

Table S1. Summary of electron mobility and its energetic disorder of PTB7:$PC_{71}BM$ BHJ films at different donor:acceptor weight ratio.

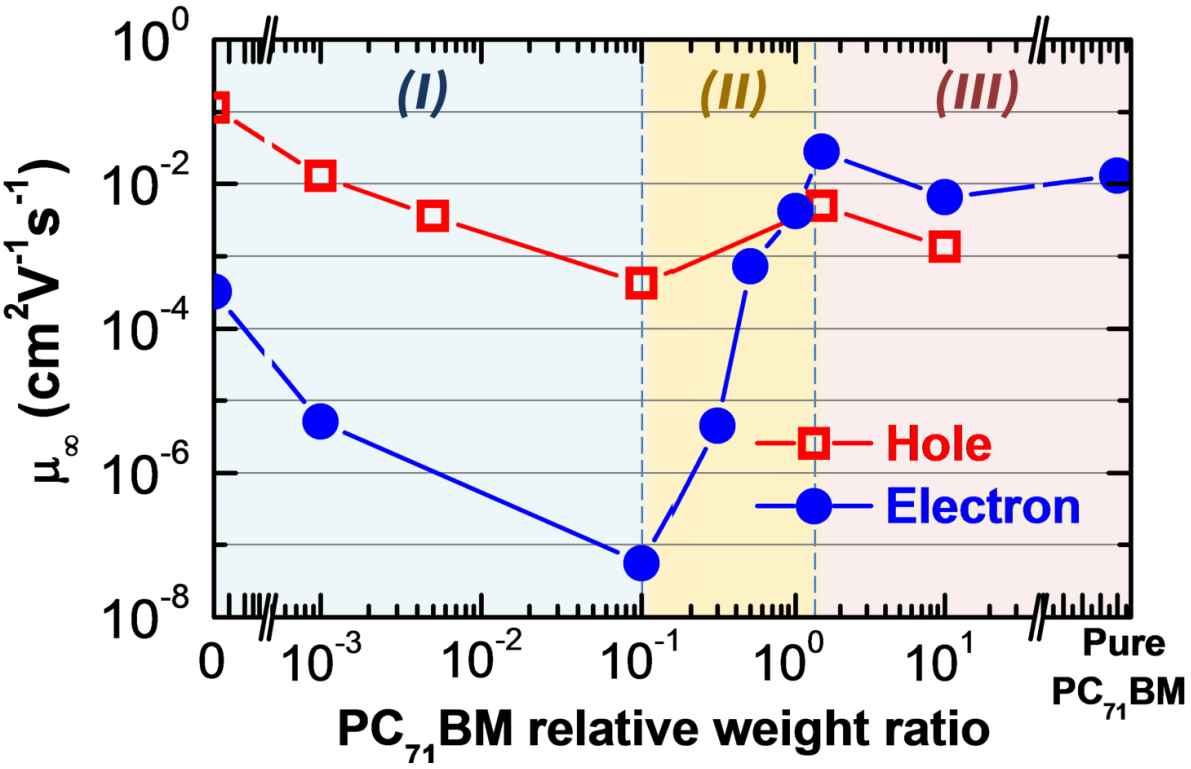

Figure S6. High temperature-limit mobilities of electron and hole at different D-A weight ratios

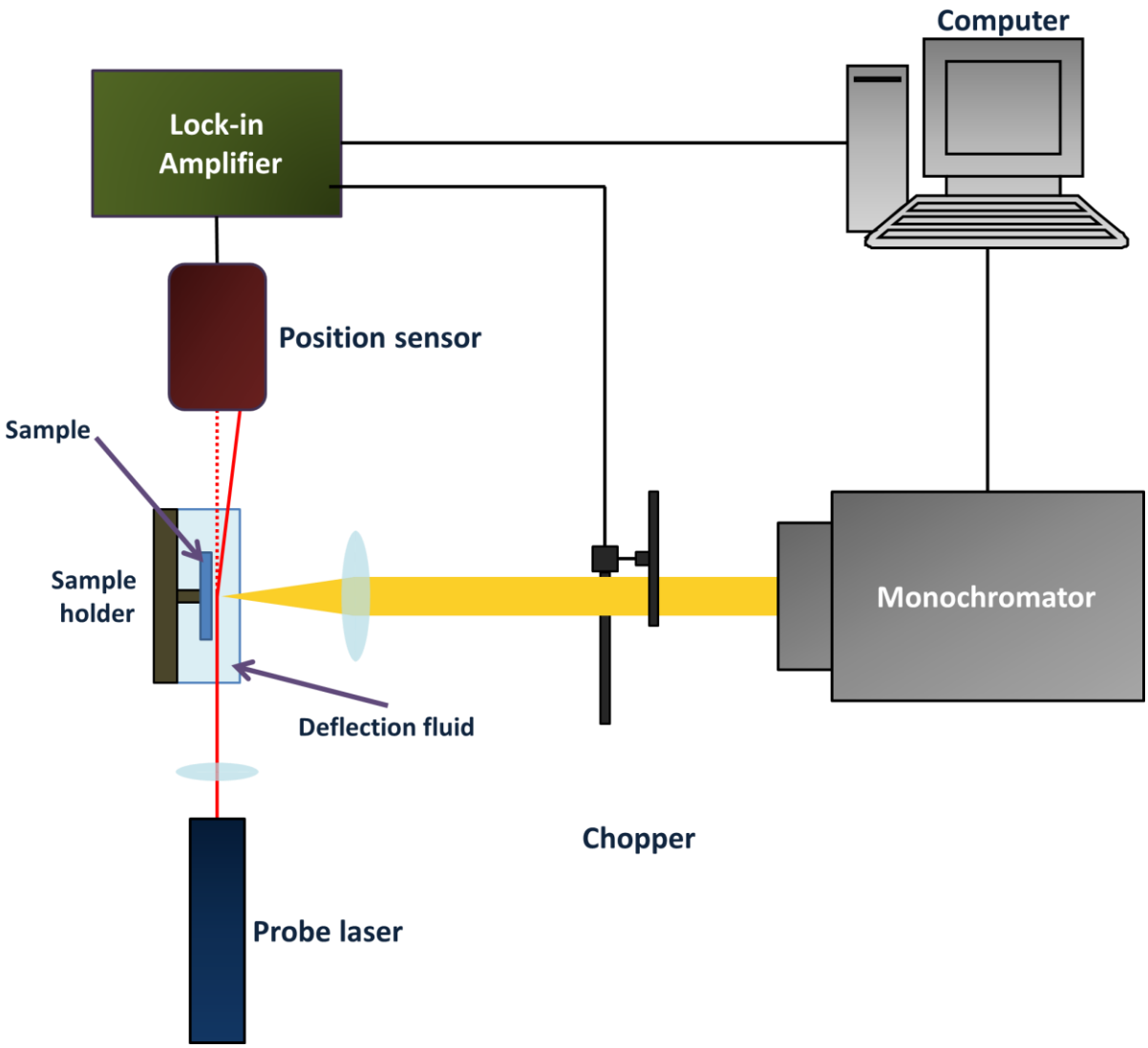

Figure S7. Experimental set-up of photothermal deflection spectroscopy. The sample under investigation was immersed in an inert, temperature sensitive deflection fluid. A mechanically chopped, wavelength tunable light source (pump beam) was shined on the surface of the sample periodically. Once there is heat released from nonradiative relaxation of photo-excited carriers at certain wavelength, the temperature rise results a periodic change in the refractive index of the fluid. A probe laser beam directed parallel to the surface of sample is used to monitor the change of refractive index, and bent proportional to the temperature gradient of the fluid near the sample surface.

Appendix: Trap density to fullerene cluster size

Molecular Density of $PC_{71}BM = 1.44 \times 10^{21}$ $cm^{-3} \approx 1 \times 10^{21}$ cm^{-3}
PTB7 molar mass = 757.11 g/mol

Mass Density of PTB7 = 1.33 g cm^{-3} (The value is from P3HT)
Molecular Density of PTB7 = 1.06×10^{21} $cm^{-3} \approx 1 \times 10^{21}$ cm^{-3}

Trap Density of pure PTB7 = 1.05×10^{18} cm^{-3}
Trap Density at 1 : 0.3 = 2.12×10^{18} cm^{-3}

Assuming

- [Trap Density at 1 : 0.3] = [Trap Density of pure PTB7] + [Trap Density from $PC_{71}BM$ clusters]
  [Trap Density from $PC_{71}BM$ clusters] = 1.07×10^{18} cm^{-3}
- Molecular density of $PC_{71}BM$ in 1 : 0.3 BHJ film $\approx (1 \times 10^{21}$ $cm^{-3}) \times 0.3 = 3 \times 10^{20}$ cm^{-3}
- Say all $PC_{71}BM$ clusters contribute to traps,
  [Number of $PC_{71}BM$ in each cluster]
  = [Molecular density of $PC_{71}BM$] / [Trap Density from $PC_{71}BM$ clusters]
  = $(3 \times 10^{20})/(1.07 \times 10^{18})$
  = 280 ($PC_{71}BM$ per cluster)
- One cluster volume = 5.04×10^{-23} m^3
- Diameter of one cluster ≈ **50 nm**

The order of diameter is in par with that reported by Ade et al.

Reference:
[1] https://www.sesres.com/physicalproperties.asp
[2] B. A. Collins, Z. Li, J. R. Tumbleston, E. Gann, C. R. McNeill, H. Ade, *Adv. Energy Mater.* **2013**, *3*, 65.